Journal of Magnetic Resonance **144,** 20–34 (2000)
doi:10.1006/jmre.2000.2024, available online at http://www.idealibrary.com on IDEAL®

Jones Matrix Formalism for Quasioptical EPR

David E. Budil,*[,1] Zhebo Ding,* Greg R. Smith,* and Keith A. Earle†

*Department of Chemistry, Northeastern University, Boston, Massachusetts 02115; and †Baker Laboratory of Chemistry and Chemical Biology, Cornell University, Ithaca, New York 14853

Received June 3, 1999; revised January 10, 2000

The Jones matrix formalism that has been used to analyze quasioptical millimeter-wave circuits is extended for specific application to high-frequency electron paramagnetic resonance (EPR). A survey of general expressions for Jones matrices of elements commonly used in quasioptical EPR spectrometers is given. The Jones matrix representations of quasioptical transmission and reflection cavities are derived, and their relationship to the equivalent circuit and transmission line representations used for conventional EPR cavities is demonstrated. The formalism is applied to selected quasioptical EPR spectrometer designs and experimental tests of the formalism are presented for two configurations of a quasioptical spectrometer operating at 220 GHz. © 2000 Academic Press

Key Words: **millimeter wave; Fabry–Perot interferometer; induction bridge; circuit analysis; Gaussian beam.**

1. INTRODUCTION

As the method of electron paramagnetic resonance (EPR) has been extended to higher frequencies and magnetic field strengths, alternative technologies have been required to replace the waveguide-based methods used at 150 GHz and below. Several groups have introduced quasioptical methods at millimeter wavelengths in increasingly complex configurations that approach the full functionality of standard EPR microwave bridges (*1–12*). The development of quasioptical EPR spectrometers has led to a need for analyzing the expected performance of such devices, as various new quasioptical equivalents for different spectrometer configurations are developed, e.g., transmission mode (*1–3*), reflection mode (*4–8*), and induction mode (*5, 6*).

One established method of analyzing quasioptical circuits at millimeter wavelengths is the Jones matrix representation (*13*), which has found general application in mm-wave spectroscopy and signal analysis. The formalism has many of the same advantages as standard circuit diagrams in characterizing and predicting the behavior of component assemblies such as mirrors, rooftop mirrors, and polarizing wire grids. In contrast, conventional EPR spectrometers have most typically been analyzed using equivalent circuits (*14*) or transmission line models (*15*), which do not explicitly treat polarization-sensitive components such as are found, for example, in an induction mode spectrometer (*5, 6, 16*). In fact, one can generalize the conventional methods of analysis to handle the more complex cases (*16*), but the method is easiest to use when only one polarization state at a time is analyzed (*17, 18*).

Martin and co-workers have made the point that many quasioptical components can be regarded as strict synonyms of the relevant components in waveguide-based microwave circuits (*19*). For example, the use of a polarization-transforming reflector as a quarter-wave transformer for transmit/receive duplexing is the quasioptical equivalent of a waveguide-based technique originally developed at microwave frequencies (*20*). This correspondence has motivated us to seek a deeper connection among equivalent circuits, transmission line analysis, and optical methods of analysis in EPR spectroscopy.

In this paper we offer an extension of the basic Jones matrix formalism developed earlier (*4, 7, 13*) that introduces a rigorous Jones matrix representation for the EPR sample cavity itself. The expressions may be related to the equivalent circuit description that is conventionally used to model EPR spectrometers and also to the impedance matrix of network and transmission line theory. The resulting formalism can be usefully integrated into a general analysis of spectrometer performance and sensitivity and can also be utilized to identify quasioptical methods for discriminating absorption from dispersion resonance signals using standard homodyne mixer detection.

Section 2 presents a brief introduction of the Jones matrix formalism and the development of new Jones matrix expressions for quasioptical transmission and reflection EPR cavities. The formalism is then applied to analyze two practical implementations of quasioptical EPR bridges in Section 3, after a brief introduction of Jones matrix expressions for the other quasioptical components required. The phase discrimination behavior predicted for these two important circuit configurations is experimentally tested in Section 4. Finally, a comparison and discussion of the results for the two configurations is given in Section 5.

[1] To whom correspondence should be addressed. Fax: (617) 373-8795. E-mail: dbudil@neu.edu.

1090-7807/00 $35.00

2. THEORY

2.1. The Jones Matrix Representation

In the Jones matrix formalism, the polarization state of the electric field of the radiation is expressed as a column vector whose elements are the components of the field along the vertical and horizontal directions:

$$\vec{\mathbf{E}} = \begin{pmatrix} E_{\mathrm{V}} \\ E_{\mathrm{H}} \end{pmatrix}. \qquad [1]$$

The horizontal direction is defined so that the unit vector $\hat{\mathbf{V}} \times \hat{\mathbf{H}}$ lies along the direction of propagation. In general, E_{V} and E_{H} are complex numbers. When they have the same phase, $\mathbf{E}$ is linearly polarized at an angle $\theta = \tan^{-1}|E_{\mathrm{H}}|/|E_{\mathrm{V}}|$ with respect to the vertical. When the phase of E_{H} differs from that of E_{V} by $-\pi/2$ or $+\pi/2$, $\mathbf{E}$ has right-hand or left-hand circular polarization, respectively.

At certain points it will also be useful to utilize a representation based on the circular polarization states:

$$\vec{\mathbf{E}} = \begin{pmatrix} E_{+} \\ E_{-} \end{pmatrix}, \qquad [2]$$

where $+$ and $-$ refer, respectively, to right- and left-hand circular polarization. The two representations are related by the transformations

$$\begin{pmatrix} E_{+} \\ E_{-} \end{pmatrix} = \frac{1}{2}\begin{pmatrix} 1 & i \\ 1 & -i \end{pmatrix}\begin{pmatrix} E_{\mathrm{V}} \\ E_{\mathrm{H}} \end{pmatrix}$$

$$\begin{pmatrix} E_{\mathrm{V}} \\ E_{\mathrm{H}} \end{pmatrix} = \begin{pmatrix} 1 & 1 \\ -i & i \end{pmatrix}\begin{pmatrix} E_{+} \\ E_{-} \end{pmatrix}. \qquad [3]$$

2.2. Jones Matrix Representation for a Quasioptical EPR Cavity

In this section, we consider two methods that have conventionally been used to represent EPR cavities, the equivalent circuit representation and the transmission line representation. The second of these is most closely related to quasioptics, since the free space propagation of a single mode such as the fundamental of a Gaussian beam lends itself to analysis by a transmission line analogy. By comparing these two methods and taking advantage of the analogy with quasioptical propagation, Jones matrices for both transmission and reflection quasioptical cavities can be derived. The transfer matrix and impedance matrix representations of transmission line elements will both be utilized in this derivation.

Equivalent circuit representation. The simplest equivalent circuit representation of a transmission cavity consists of an ideal transformer with an n_1:1 turns ratio at the input, a series RLC circuit representing the cavity plus sample, and an ideal transformer with a 1:n_2 turns ratio at the output, as shown in Fig. 1a (*14, 21*).

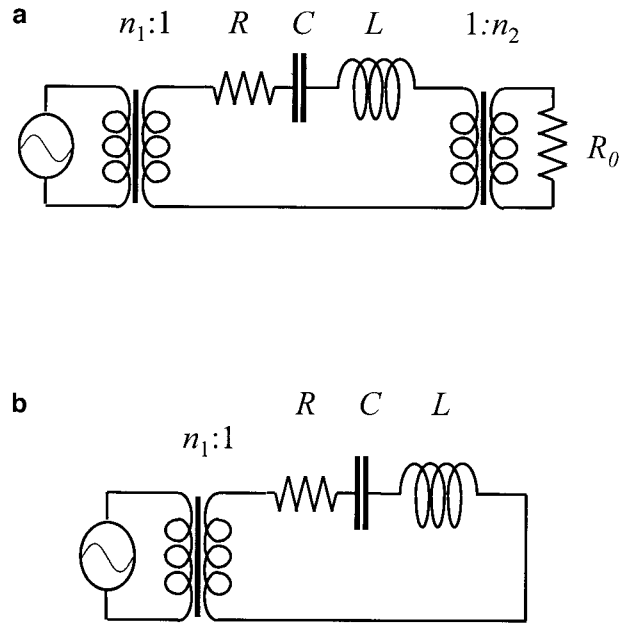

FIG. 1. Equivalent electrical circuit representations for (a) a transmission cavity and (b) a reflection cavity.

Assuming that the cavity reactance X can be represented by an effective inductance and an effective capacitance in series,

$$X = \omega L - \frac{1}{\omega C} = \omega_0 L\left(\frac{\omega}{\omega_0} - \frac{\omega_0}{\omega}\right), \qquad [4]$$

where $\omega_0 = 1/\sqrt{LC}$ is the resonant frequency of the cavity. The unloaded quality factor of the cavity is

$$Q_{\mathrm{U}} = \frac{\omega_0 L}{R}. \qquad [5]$$

If we define the coupling parameters,

$$\beta_1 = \frac{Z_0}{n_1^2 R}; \quad \beta_2 = \frac{Z_0}{n_2^2 R}, \qquad [6]$$

then the loaded and radiation Q factors of the cavity are, respectively, given by

$$Q_{\mathrm{L}} = \frac{Q_{\mathrm{U}}}{1 + \beta_1 + \beta_2}$$

$$Q_{\mathrm{R}} = \frac{Q_{\mathrm{U}}}{\beta_1 + \beta_2}, \qquad [7]$$

and the power transmitted, reflected, and absorbed by the resonator circuit is

$$T = \frac{4\beta_1\beta_2}{\Delta} \quad [8]$$

$$R = 1 - \frac{4\beta_1(\beta_2 + 1)}{\Delta} \quad [9]$$

$$A = \frac{4\beta_1}{\Delta}, \quad [10]$$

where

$$\Delta = (1 + \beta_1 + \beta_2)^2 + Q_U^2\left(\frac{\omega}{\omega_0} - \frac{\omega_0}{\omega}\right)^2. \quad [11]$$

Analogous results for the reflection mode circuit shown in Fig. 1b can be obtained by allowing $\beta_2 \rightarrow 0$ in the above expressions, in which case the transmitted power is zero and the resonance properties of the cavity are determined from the reflected power.

Transfer matrix representation. We now seek to demonstrate the equivalence of this circuit with a quasioptical cavity such as a Fabry–Perot interferometer containing a paramagnetic dielectric layer. A convenient means to accomplish this is the transmission line transfer matrix representation (*22*) since transmission lines can be used to represent both microwave circuits and the propagation of a single wave mode through dielectric layers (*23*).

The transfer matrix relates the input and output voltages and currents of a linear two-port device as

$$\begin{pmatrix} V_{in} \\ I_{in} \end{pmatrix} = \mathbf{M}\begin{pmatrix} V_{out} \\ I_{out} \end{pmatrix} = \begin{pmatrix} A & B \\ C & D \end{pmatrix}\begin{pmatrix} V_{out} \\ I_{out} \end{pmatrix}. \quad [12]$$

For reciprocal devices, $AD - BC = 1$, and for symmetric devices $A = D$. A useful property of this representation is that the output current and voltage for a given element are equal to the input current and voltage of the next element. Thus, a series of optical or circuit elements may be represented by successive multiplication of the matrices for each element.

The field reflection and transmission coefficients for a given transfer matrix are given by

$$r = \frac{AZ_{out} + B - CZ_{in}Z_{out} - DZ_{in}}{AZ_{out} + B + CZ_{in}Z_{out} + DZ_{in}}$$

$$t = \frac{2Z_{out}}{AZ_{out} + B + CZ_{in}Z_{out} + DZ_{in}}, \quad [13]$$

where Z_{in} and Z_{out} are the input and output impedances.

To find the system transfer matrix equivalent for the circuits shown in Fig. 1, the matrix representations for the n:1 ideal transformer and for a series impedance Z are required (*24*),

$$\mathbf{M}_{n:1} = \begin{pmatrix} n & 0 \\ 0 & 1/n \end{pmatrix}$$

$$\mathbf{M}_{series}(Z) = \begin{pmatrix} 1 & Z \\ 0 & 1 \end{pmatrix}, \quad [14]$$

which give for the circuit

$$\mathbf{M}_{cir} = \begin{pmatrix} n_1 & 0 \\ 0 & 1/n_1 \end{pmatrix}\begin{pmatrix} 1 & R + iX \\ 0 & 1 \end{pmatrix}\begin{pmatrix} 1/n_2 & 0 \\ 0 & n_2 \end{pmatrix}$$

$$= \begin{pmatrix} n_1/n_2 & n_1n_2(R + iX) \\ 0 & n_2/n_1 \end{pmatrix}. \quad [15]$$

Equations [4] through [6] may be substituted into the above expression to give the transfer matrix in terms of the equivalent circuit parameters:

$$\mathbf{M}_{cir} = \begin{pmatrix} \sqrt{\frac{\beta_1}{\beta_2}} & \frac{Z_0}{\sqrt{\beta_1\beta_2}}\left(1 + iQ_U\left(\frac{\omega}{\omega_0} - \frac{\omega_0}{\omega}\right)\right) \\ 0 & \sqrt{\frac{\beta_2}{\beta_1}} \end{pmatrix}. \quad [16]$$

It is straightforward to verify that Eqs. [8] through [10] follow directly from application of Eqs. [13] to the above matrix with input and output impedance equal to Z_0, using the definitions for power transmission, reflection, and absorption in terms of the field coefficients: $T = |t|^2$, $R = |r|^2$, and $A = 1 - (T + R)$.

Transfer matrix representation of a quasioptical EPR cavity. To represent a simple quasioptical cavity such as a Fabry–Perot interferometer filled with a dielectric, two more representative matrices are required. A coupling element such as partially reflective wire mesh or iris may be represented as a shunt element of impedance Z_g (*13, 25, 26*) on a transmission line, which has the transfer matrix (*17, 20*)

$$\mathbf{M}_{shunt}(Z_s) = \begin{pmatrix} 1 & 0 \\ 1/Z_s & 1 \end{pmatrix}. \quad [17]$$

Application of the second of Eqs. [13] to this matrix gives a result consistent with standard expressions for the mirror reflectivity (*26*). Typically, one assumes that Z_g is purely reactive (i.e., $Z_g = -iX_g$) and small (*25*), although this formalism can handle small losses due to such effects as diffraction from an iris or resistive losses in the metal of the mirror.

The transfer matrix for a slab of dielectric of thickness d and impedance $Z = \sqrt{\mu/\epsilon}$ is

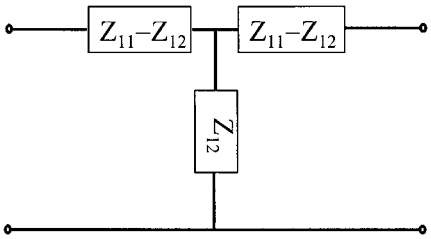

FIG. 2. Equivalent impedance "T"-network for a reciprocal two-port device on a transmission line.

$$\mathbf{M}_{\text{diel}} = \begin{pmatrix} \cosh \gamma d & Z \sinh \gamma d \\ \dfrac{1}{Z} \sinh \gamma d & \cosh \gamma d \end{pmatrix}, \qquad [18]$$

where $\gamma = ik_0\sqrt{\mu\epsilon}$, $k_0 = 2\pi/\lambda_0$ is the wave number of the radiation in free space, $\epsilon = \epsilon' + i\epsilon''$ is the permittivity of the medium, and $\mu = \mu_0(1 + \chi)$ is its permeability. In the absence of an EPR resonance, $\mu = 1$, and the complex components of $\gamma = \alpha + i\beta$ may be expressed as

$$\alpha = k_0 \text{Im}\{\sqrt{\epsilon}\} = k_0\sqrt{(\sqrt{\epsilon'^2 + \epsilon''^2} - \epsilon')/2} = \frac{k_0\epsilon''}{2\ \text{Re}\{\sqrt{\epsilon}\}}$$

$$\beta = k_0 \text{Re}\{\sqrt{\epsilon}\} = k_0\sqrt{(\sqrt{\epsilon'^2 + \epsilon''^2} + \epsilon')/2}. \qquad [19]$$

In order to demonstrate the equivalence of $\mathbf{M}_{\text{shunt}}$ to an ideal n:1 transformer and that between $\mathbf{M}_{\text{diel}}$ and a series impedance, it is convenient to utilize an alternative representation for reciprocal two-port devices known as the impedance or **Z**-matrix (*17, 22*). This representation relates the input and output currents and voltages of the device as

$$\begin{pmatrix} V_{\text{in}} \\ V_{\text{out}} \end{pmatrix} = \mathbf{Z}\begin{pmatrix} I_{\text{in}} \\ I_{\text{out}} \end{pmatrix} = \begin{pmatrix} Z_{11} & Z_{12} \\ Z_{21} & Z_{22} \end{pmatrix}\begin{pmatrix} I_{\text{in}} \\ I_{\text{out}} \end{pmatrix}. \qquad [20]$$

In terms of the elements of **M** for a given system, **Z** is given by

$$\mathbf{Z} = \begin{pmatrix} A/C & (AD - BC)/C \\ 1/C & A/C \end{pmatrix} = \begin{pmatrix} A/C & 1/C \\ 1/C & A/C \end{pmatrix}. \qquad [21]$$

Because of the property $AD - BC = 1$, $Z_{21} = Z_{12}$ and the device may be represented by the equivalent "T-network" shown in Fig. 2. Transformation between equivalent representations of a given device is then accomplished by equating the elements of the **Z** matrices corresponding to each representation.

In particular, a shunt impedance may be represented by an equivalent circuit consisting of a length of lossless transmission line of characteristic impedance Z_0 followed by an ideal n_1:1 transformer (*22*). When the real part of the propagation constant γ for the transmission line is zero, the transfer matrix for this equivalent circuit is

$$\begin{pmatrix} n_1\cos(k_0 d) & \dfrac{iZ_0}{n_1}\sin(\beta d) \\ \dfrac{in_1}{Z_0}\sin(\beta d) & \dfrac{\cos(\beta d)}{n_1} \end{pmatrix}. \qquad [22]$$

Thus, applying Eq. [21] to Eq. [22] and to Eq. [17] with $Z_g = -iX_g$ one obtains

$$\begin{pmatrix} iX_m & iX_m \\ iX_m & iX_m \end{pmatrix} = \begin{pmatrix} iZ_0\cot\beta d & i\dfrac{Z_0}{n_1}\csc\beta d \\ i\dfrac{Z_0}{n_1}\csc\beta d & i\dfrac{Z_0}{n_1^2}\cot\beta d \end{pmatrix}, \qquad [23]$$

which has the solution $\beta d = \cos^{-1}(1/n_1)$, $n_1 = Z_0/(X_g \sin \beta d)$. For large n_1, $\beta d \to \pi/2$ and $n_1 \to Z_0/X_g$; i.e., the grid becomes equivalent to an ideal n_1:1 transformer followed by a quarter-wave transmission line. Similarly, the shunt impedance of the second mirror can be shown to be equivalent to a quarter-wave transmission line followed by an ideal $1{:}n_2$ transformer. The net addition of a half-wavelength of transmission line between the mirrors leaves the effective impedance of the dielectric medium inside the cavity unchanged.

The matrix $\mathbf{M}_{\text{diel}}$ may be transformed into an equivalent series impedance by adjusting d so that $\text{Im}\{\sinh \gamma d\} = 0$ (this corresponds to the resonance condition $\beta d = m\pi$). The effective series impedance Z_{eff} at resonance may not be determined by directly comparing Eq. [18] with Eq. [15] since Z in Eq. [18] becomes indeterminate when $\sinh \gamma d = 0$. In terms of the **Z** matrix, this condition corresponds to $Z_{12} \to \infty$, which effectively removes the shunt impedance from the T-network. It is readily seen from Fig. 2 that maximum transfer of power through the T-network occurs when the short circuit is removed, and the effective series impedance of the network will be $(Z_{11} + Z_{22} - 2Z_{12})$. Application of Eq. [21] to Eq. [18] allows the series impedance to be written in terms of the dielectric properties,

$$\begin{aligned} Z_{\text{eff}} &= 2(Z_{11} - Z_{12}) \\ &= i2Z\,\frac{\cosh(\gamma d) - 1}{\sinh(\gamma d)} \\ &= i2Z\tanh\frac{\gamma d}{2} \\ &= i2Z\tanh \alpha d, \end{aligned} \qquad [24]$$

where the final step makes use of the resonance condition $\beta d = m\pi$. Note that for a lossless dielectric, $Z_{\text{eff}} = 0$ and the dielectric slab becomes a perfect "absentee layer" at resonance. For relatively low-loss material, one may make the approximation $\tanh \alpha d \approx \alpha d$. Then, in the absence of an EPR resonance (i.e., for $\mu = 1$) one may write

$$i2dZ\alpha = i2d\,\frac{\alpha}{\sqrt{\epsilon}} = i2dk_0\,\frac{\alpha}{\alpha + i\beta}, \qquad [25]$$

which leads to an expression for the effective Q_U of the dielectric layer:

$$Q_U = \frac{\mathrm{Im}\{Z_{\mathrm{eff}}\}}{\mathrm{Re}\{Z_{\mathrm{eff}}\}} = \frac{\beta}{\alpha} = \frac{\epsilon' - |\epsilon|/2}{\epsilon''} \approx \frac{\epsilon'}{2\epsilon''}, \qquad [26]$$

where the last step applies the approximation $\epsilon''^2 \ll \epsilon'^2$, valid for low-loss material. Thus it has been shown that the equivalent circuit parameters conventionally used to describe EPR cavities may be expressed in terms of the electromagnetic properties of a dielectric-filled Fabry–Perot interferometer.

The Jones matrix representation of the quasioptical EPR cavity can now be constructed from the field transmission and reflection coefficients obtained by applying Eqs. [13] to the transfer matrix in Eq. [16]:

$$t = \frac{\sqrt{\beta_1\beta_2}}{(1 + \beta_1 + \beta_2) - iQ_U\left(\dfrac{\omega}{\omega_0} - \dfrac{\omega_0}{\omega}\right)} \qquad [27]$$

and

$$r = \frac{(1 - \beta_1 + \beta_2) - iQ_U\left(\dfrac{\omega}{\omega_0} - \dfrac{\omega_0}{\omega}\right)}{(1 + \beta_1 + \beta_2) - iQ_U\left(\dfrac{\omega}{\omega_0} - \dfrac{\omega_0}{\omega}\right)}. \qquad [28]$$

Equation [26] makes explicit the fact that Q_U depends only on the dielectric properties of the medium, as do the coupling parameters β_1 and β_2 to a good approximation. Thus, an EPR resonance will affect the transmitted and reflected fields only through its effect on ω, which depends in turn upon the effective index of refraction, $n = (\mu\epsilon)^{1/2}$ as

$$\omega = \frac{2\pi nc}{\lambda_0}. \qquad [29]$$

Note that ω and n are in general complex quantities. An EPR resonance will change the permeability by an amount $\delta\mu = \chi$, so that

$$\delta\omega = \left(\frac{\partial\omega}{\partial\mu}\right)\delta\mu = \frac{2\pi c}{\lambda_0}\left(\frac{1}{2}\right)\frac{\epsilon}{\sqrt{\mu\epsilon}}\,\chi \approx \frac{\omega_0\chi}{2}, \qquad [30]$$

where the last step includes the approximations $n \approx 1/Z$ and $\omega \approx \omega_0$.

Away from magnetic resonance, $\omega = \omega_0$, and

$$t = \frac{T}{A} = \frac{2\sqrt{\beta_1\beta_2}}{(1 + \beta_1 + \beta_2)}$$

$$r = \frac{R}{A} = \frac{(1 - \beta_1 + \beta_2)}{(1 + \beta_1 + \beta_2)} = 1 - \frac{2\beta_1}{(1 + \beta_1 + \beta_2)}. \qquad [31]$$

If the cavity is detuned to $\omega = \omega_0 + \delta\omega$ by the EPR resonance and a fraction η of the sample volume is EPR active, the transmission and reflection coefficients become

$$t + \delta t = \frac{2\sqrt{\beta_1\beta_2}}{(1 + \beta_1 + \beta_2) - iQ_U\dfrac{2\delta\omega}{\omega_0}}$$

$$= \frac{2\sqrt{\beta_1\beta_2}}{(1 + \beta_1 + \beta_2)}(1 - i\eta Q_L\chi)$$

$$r + \delta r = \frac{(1 - \beta_1 + \beta_2) - iQ_U\dfrac{2\delta\omega}{\omega_0}}{(1 + \beta_1 + \beta_2) - iQ_U\dfrac{2\delta\omega}{\omega_0}}$$

$$= \frac{(1 - \beta_1 + \beta_2) + 2i\beta_1\eta Q_L\chi}{(1 + \beta_1 + \beta_2)}, \qquad [32]$$

which are consistent with the standard results (*27*).

Equations [32] are written for an unspecified polarization state of the resonant radiation. In fact, for radiation propagating along the spectrometer field direction, χ is only significant for one sense of circular polarization, say the positive one, and is essentially zero for the opposite sense. Thus, Eqs. [32] can be used to construct a Jones matrix in the circularly polarized basis:

$$\begin{pmatrix} T_+ \\ T_- \end{pmatrix} = \frac{2\sqrt{\beta_1\beta_2}}{(1 + \beta_1 + \beta_2)}\begin{pmatrix} 1 - i\eta Q_L\chi & 0 \\ 0 & 1 \end{pmatrix}\begin{pmatrix} A_+ \\ A_- \end{pmatrix}$$

$$\begin{pmatrix} R_+ \\ R_- \end{pmatrix} = \frac{1}{(1 + \beta_1 + \beta_2)}$$

$$\times\begin{pmatrix} (1 - \beta_1 + \beta_2) + 2i\beta_1\eta Q_L\chi & 0 \\ 0 & (1 - \beta_1 + \beta_2) \end{pmatrix}$$

$$\times\begin{pmatrix} A_+ \\ A_- \end{pmatrix}. \qquad [33]$$

This is readily transformed into the linearly polarized basis set according to Eqs. [3]:

$$\begin{pmatrix} T_V \\ T_H \end{pmatrix} = \frac{\sqrt{\beta_1\beta_2}}{(1+\beta_1+\beta_2)} \begin{pmatrix} 1-i\eta Q_L\chi & \eta Q_L\chi \\ -\eta Q_L\chi & 1-i\eta Q_L\chi \end{pmatrix} \begin{pmatrix} A_V \\ A_H \end{pmatrix}$$

$$\begin{pmatrix} R_V \\ R_H \end{pmatrix} = \frac{1}{(1+\beta_1+\beta_2)} \begin{pmatrix} (1-\beta_1+\beta_2)+i\beta_1\eta Q_L\chi & -\beta_1\eta Q_L\chi \\ -\beta_1\eta Q_L\chi & -(1-\beta_1+\beta_2)-i\beta_1\eta Q_L\chi \end{pmatrix} \begin{pmatrix} A_V \\ A_H \end{pmatrix}. \quad [34]$$

The first of these equations contains the Jones matrix for a transmission mode cavity, where the quantities of interest are the transmitted fields. The second of Eqs. [34] gives the fields reflected from the cavity, adjusted for the sign convention of the horizontal component. This expression makes clear that the EPR signal can be measured in the beam reflected from the cavity as well as in the transmitted beam. To obtain the Jones matrix for a reflection cavity, one sets $\beta_2 = 0$ in the second of Eqs. [34], leaving a single coupling parameter β.

$$\begin{pmatrix} R_V \\ R_H \end{pmatrix} = \frac{1}{(1+\beta)} \times \begin{pmatrix} (1-\beta)+i\beta\eta Q_L\chi & -\beta\eta Q_L\chi \\ -\beta\eta Q_L\chi & -(1-\beta)-i\beta\eta Q_L\chi \end{pmatrix} \times \begin{pmatrix} A_V \\ A_H \end{pmatrix} \quad [35]$$

This matrix is defined so that "output" of the cavity gives the reflected fields according to the convention for the sign of the horizontal field.

2.3. Jones Matrices for Other Quasioptical Components

We now introduce Jones matrices for the other quasioptical components that will be utilized in the quasioptical EPR spectrometer circuits discussed below. A more complete survey of Jones matrices for general quasioptical applications has been given by Lesurf (*13*).

Mirror. The Jones matrix for an ideal planar reflector is given by

$$\mathbf{M} = \begin{pmatrix} R_V \\ R_H \end{pmatrix} = \begin{pmatrix} -1 & 0 \\ 0 & 1 \end{pmatrix} \begin{pmatrix} E_V \\ E_H \end{pmatrix}. \quad [36]$$

Because the tangential component of the electric field must vanish at the surface of a conductor, the reflected fields are rotated by π relative to the incident fields; the expression above takes into account the convention for the positive H direction of the reflected beam.

Wire grid. A wire grid with appropriate wire diameter and spacing will reflect the E field component that is parallel to the direction of the wires and transmit the orthogonal component (*28*). For fields along the wire direction, the grid will invert the field of the reflected radiation in the same way as a regular mirror. In the frame with the wires along the vertical axis, the Jones matrices for reflection and transmission are therefore

$$\begin{pmatrix} R_V \\ R_H \end{pmatrix} = \mathbf{G}_R \begin{pmatrix} E_V \\ E_H \end{pmatrix} = \begin{pmatrix} -1 & 0 \\ 0 & 0 \end{pmatrix} \begin{pmatrix} R_V \\ R_H \end{pmatrix}$$

$$\begin{pmatrix} R_V \\ R_H \end{pmatrix} = \mathbf{G}_T \begin{pmatrix} E_V \\ E_H \end{pmatrix} = \begin{pmatrix} 0 & 0 \\ 0 & 1 \end{pmatrix} \begin{pmatrix} E_V \\ E_H \end{pmatrix}. \quad [37]$$

If the grid is placed at an angle of θ relative to the vertical, as in the configurations discussed below, the reflection and transmission matrices become

$$\mathbf{G}_R(\theta) = \begin{pmatrix} \cos\theta & -\sin\theta \\ \sin\theta & \cos\theta \end{pmatrix} \begin{pmatrix} -1 & 0 \\ 0 & 0 \end{pmatrix} \begin{pmatrix} \cos\theta & -\sin\theta \\ \sin\theta & \cos\theta \end{pmatrix} = \begin{pmatrix} -\cos^2\theta & -\cos\theta\sin\theta \\ \cos\theta\sin\theta & \sin^2\theta \end{pmatrix}$$

$$\mathbf{G}_T(\theta) = \begin{pmatrix} \cos\theta & \sin\theta \\ -\sin\theta & \cos\theta \end{pmatrix} \begin{pmatrix} 0 & 0 \\ 0 & 1 \end{pmatrix} \begin{pmatrix} \cos\theta & -\sin\theta \\ \sin\theta & \cos\theta \end{pmatrix} = \begin{pmatrix} \cos^2\theta & -\cos\theta\sin\theta \\ -\cos\theta\sin\theta & \sin^2\theta \end{pmatrix}. \quad [38]$$

Rooftop mirror. The rooftop mirror consists of two planar mirrors at a right angle to each other. The axis common to both planes is placed perpendicular to the direction of beam propagation. For E fields parallel to the axis, two reflections of the incident beam leave the vector orientation unchanged. For E fields perpendicular to the axis, the output vector is rotated by an angle of π from the input vector. Thus, if the incident E field is at an angle of $\pi/4$, the combined reflections result in a net rotation of the polarization direction by $\pi/2$. In the frame where the rooftop axis is vertical, the Jones matrix is simply the unit matrix, taking into account the convention for the positive H direction of the reflected radiation. When the axis is placed at an arbitrary angle θ with respect to the vertical, the Jones matrix is given by

$$\mathbf{R}_R(\theta) = \begin{pmatrix} \cos^2\theta - \sin^2\theta & -2\cos\theta\sin \\ -2\cos\theta\sin\theta & \cos^2\theta - \sin^2\theta \end{pmatrix}. \quad [39]$$

Free-space propagation. The phase change due to travel of a wave through a distance d in space may be represented by the matrix

$$\Phi(d) = \exp\left(\frac{2\pi d}{\lambda}\right)\begin{pmatrix}1 & 0\\ 0 & 1\end{pmatrix}. \quad [40]$$

Most typically this matrix is explicitly included in a quasioptical circuit in order to represent the difference in distances traveled over two paths in the quasioptical circuit.

3. APPLICATION OF THE JONES MATRIX FORMALISM

3.1. General Procedure for Analyzing EPR Circuits

We now proceed to examine Jones matrix representations for the two quasioptical EPR circuits that are most commonly used above 150 GHz, namely a simple transmission mode spectrometer and an induction mode spectrometer utilizing a reflection cavity. As usual for cw EPR, it will be assumed that the Zeeman field is modulated at a frequency ω_m and a phase-sensitive detection scheme (lock-in amplifier) is used to filter the signal at the same frequency.

For an arbitrary lineshape function $f(\xi)$ that is analytic over an appropriate interval around the point $\xi = x$, one may apply the Taylor expansion to obtain the time-dependent signal (*29*)

$$f(x + h\sin\omega_m t) = \sum_{n=0}^{\infty} h^n \sin^n\omega_m t\left(\frac{1}{n!}\frac{d^n f(x)}{dx^n}\right). \quad [41]$$

For simplicity of presentation, only terms up to first order in sin $\omega_m t$ will be retained from Eq. [41]. This will allow the essential features of phase-sensitive detection to be illustrated for the two circuit geometries.

By analogy with waveguide-based EPR, phase discrimination requires a mixer in which the detector is illuminated by the EPR signal and a reference signal in such a way that the relative phases of the two signals can be controlled. In the following discussion, the effect of the dc bias provided by the reference or carrier signals will be neglected, since many of the commercially available detectors at mm-wave frequencies are internally biased. However, the formalism does allow an evaluation of the bias, and it is possible in principle to vary the RF bias level for several of the designs discussed below.

The transmission mode circuit discussed below may also include a polarizing element in front of the detector. Such an element is intrinsic to rectangular waveguide-mounted detectors, since the waveguide functions essentially the same way as a wire grid reflector with the wires parallel to the broad face of the waveguide. The same functionality can be achieved by placing a wire grid in front of nonpolarizing detectors such as bolometers.

In order to clarify the results for each circuit, terms will be collected in the matrices for transmission and reflection cavities

$$\mathbf{C}_T = \begin{pmatrix} a_T - ib_T z & b_T z \\ -b_T z & a_T - ib_T z \end{pmatrix}$$

$$\mathbf{C}_R = \begin{pmatrix} a_R + ib_R z & -b_R z \\ -b_R z & -a_R - ib_R z \end{pmatrix}, \quad [42]$$

where

$$a_T = \frac{2\sqrt{\beta_1\beta_2}}{1+\beta_1+\beta_2}; \quad b_T = a_T\eta Q_L$$

$$a_R = \frac{1-\beta_1}{1+\beta_1}; \quad b_R = \frac{\beta_1}{1+\beta_1}\eta Q_L \quad [43]$$

and

$$z = z' + iz'' = ((\chi')^{(1)} + i(\chi'')^{(1)})\sin\omega_m t, \quad [44]$$

in which the superscript indicates the first derivative of the susceptibility function with respect to frequency. Thus, a_T gives the magnitude of the "carrier" power and b_T represents the signal amplification due to the cavity.

3.2. Transmission Spectrometer

The circuit for a simple transmission cavity arrangement (i.e., source–cavity–detector) with a vertically polarized source is

$$\mathbf{C}_T\mathbf{V} = \begin{pmatrix} a_T + ib_T z \\ -b_T z \end{pmatrix}. \quad [45]$$

A nonpolarizing detector such as a bolometer will measure the sum of the vertical and horizontal field amplitudes, producing a signal given (after substituting Eq. [44]) by

$$a_T^2 - 2a_T b_T \sin\omega_m t(\chi'') + 2b_T^2\sin^2\omega_m t((\chi'^{(1)})^2 + (\chi''^{(1)})^2). \quad [46]$$

If a polarizer is placed in front of the detector so as to admit the electric field component that is oriented at an angle θ with respect to the vertical, the incident electric field is the weighted sum of the vertical and horizontal components given in Eq. [45]:

$$\begin{aligned} E_\theta &= \cos\theta(a_T + b_T z) - \sin\theta(ib_T z) \\ &= \cos\theta(a_T + b_T\sin\omega_m t(\chi''^{(1)} + i\chi'^{(1)})) \\ &\quad - \sin\theta(b_T\sin\omega_m t(\chi''^{(1)} + i\chi'^{(1)})). \end{aligned} \quad [47]$$

The power detected will be proportional to the squared amplitude of this field,

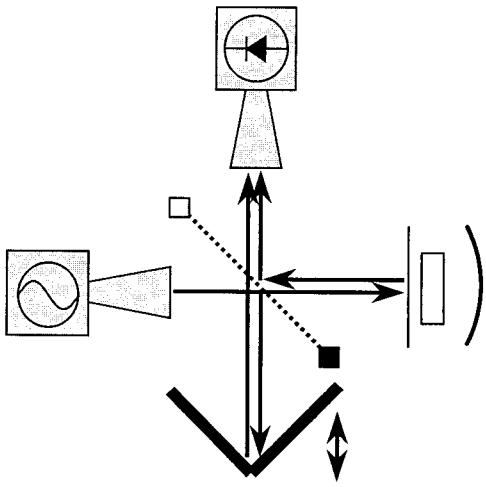

FIG. 3. Circuit diagram of the induction mode spectrometer configuration based on a central wire grid with a moveable rooftop mirror in the reference arm that enables phase adjustment of the reference signal.

$$|E_\theta|^2 = a_T^2\cos^2\theta + a_T b_T[(\cos 2\theta + 1)\chi''^{(1)} - \sin 2\theta\chi'^{(1)}] \times \sin\theta_m t + b_{TL}^2[((\chi'^{(1)})^2 + (\chi''^{(1)})^2)]\sin^2\omega_m t. \quad [48]$$

This result demonstrates how the detector polarization leads to phase discrimination of the EPR signal in the simple transmission mode. The first, time-independent term represents the transmitted source power at the detector, which depends upon the detector orientation. More importantly, the $\sin(\omega_m t)$ term contains both absorption and dispersion terms, which are weighted according to the detector angle. There is a half-angle relationship between the detector angle and the phase angle that determines the amount of absorption and dispersion in the observed spectrum. This arises from the $\cos^2\theta$ dependence of the detected power on the orientation angle of the detector.

3.3. Induction Spectrometer

In order to recover phase information while operating with a reflection cavity, it is necessary to divert some of the source power into a reference arm, by analogy with conventional waveguide-based EPR bridges. Typically a polarizing wire grid is used for this purpose, although a nonpolarizing dielectric beam splitter may also be utilized. The beams reflected from the reference arm and the sample cavity are recombined in the detector with a phase difference that is controlled by changing the relative path lengths of the two beams. One example of such a circuit is the induction mode spectrometer, shown in Fig. 3. This circuit must be represented by the sum of two matrix products representing the paths along the sample and reference arms.

In reflection cavity designs, it is also worth noting that optical components oriented with a rotation angle of θ with respect to the incident radiation present a rotation angle of $-\theta$ to the reflected radiation because of the convention defining the H direction. Thus, the grid appears first as $\mathbf{G}_T(\pi/4)$ and then as $\mathbf{G}_R(-(\pi/4))$ in the matrix product describing the path that goes through the cavity shown in Fig. 3.

In its simplest implementation, the induction mode spectrometer resembles a standard polarizing interferometer (*30*), with the exception that there is no quarter-wave transformer between the sample arm and the polarizing grid. The source power is divided into two paths. In the first path, the component of the initially vertically polarized radiation that is transmitted through the grid is not rotated upon reflection from the cavity and thus passes back through the grid toward the source. However, one of the linearly polarized components of the circularly polarized EPR signal is reflected by the grid into the detector. In the second path, the component that is initially reflected from the grid is directed onto a rooftop mirror, rotated by $\pi/2$, transmitted by the grid, and combined with the EPR signal at the detector. The phase difference between the two waves determines the phase of the measured EPR signal. This is controlled by adjusting the rooftop mirror position to vary the difference in path lengths between the sample and reference arms. The sum of the two paths is

$$\left[\left(\mathbf{G}_T\left(\frac{\pi}{4}\right)\Phi(\phi)\mathbf{R}_R(0)\mathbf{G}_R\left(\frac{\pi}{4}\right)\right) + \left(\mathbf{G}_R\left(-\frac{\pi}{4}\right)\mathbf{C}_R\mathbf{G}_T\left(\frac{\pi}{4}\right)\right)\right]\mathbf{V} = \frac{1}{2}\begin{pmatrix} -e^{-\phi} & -b_R z \\ e^{i\phi} & -b_R z \end{pmatrix}, \quad [49]$$

which gives the signals for a vertically polarized detector,

$$|E_V|^2 = \frac{1}{4} + \frac{b_R}{2}[\cos\phi\chi'^{(1)} - \sin\phi\chi''^{(1)}]\sin\omega_m t + \frac{b_R^2}{4}((\chi'^{(1)})^2 + (\chi''^{(1)})^2)\sin^2\omega_m t, \quad [50]$$

and for a horizontally polarized detector,

$$|E_H|^2 = \frac{1}{4} - \frac{b_R}{2}[\cos\phi\chi'^{(1)} - \sin\phi\chi''^{(1)}]\sin\omega_m t + \frac{b_R^2}{4}((\chi'^{(1)})^2 + (\chi''^{(1)})^2)\sin^2\omega_m t. \quad [51]$$

4. EXPERIMENTAL

We now present experimental tests of the signal phase behavior predicted by the Jones matrix formalism for the two spectrometer configurations detailed in the last section. Since the scales of the absorption and dispersion components of an

EPR signal are related by the Hilbert transform (i.e., the Kramers–Krönig relations), the phase of an arbitrary signal may be measured by determining the relative contributions of absorption and dispersion in the spectrum. This is most conveniently accomplished when both the absorption and the dispersion lineshapes are well represented by analytical expressions such as the Lorentzian function. In this case, the relative amounts of absorption and dispersion may be determined by least-squares analysis of the experimental spectrum.

A standard sample of 1 mM Tempone in undegassed toluene solution was chosen for this analysis. This probe produces a motionally averaged three-line spectrum typical of nitroxides at ambient temperatures. At 220 GHz, rotational spin relaxation and line-broadening due to dissolved oxygen produce a lineshape that is very well approximated by the Lorentzian function. The experimental spectra were fitted by Levenberg–Marquardt nonlinear least-squares with a linear combination of Lorentzian absorption and dispersion lineshapes given by the function

$$g(x) = \sum_{m=1}^{3} \left[a_{\mathrm{A}} \frac{-2b_m(x - c_m)}{((x - c_m)^2 + b_m^2)^2} + a_{\mathrm{D}} \frac{(b_m^2 - (x - c_m)^2)}{((x - c_m)^2 + b_m^2)^2} \right]. \quad [52]$$

The fitting parameters include a_{A}, the amplitude of the absorption component; a_{D}, that of the dispersion; b_m, the Lorentzian linewidth (i.e., the inverse homogeneous T_2) of the mth line; and c_m, the field position of the mth line.

The locally constructed quasioptical 220-GHz spectrometer used to obtain the experimental spectra has been described elsewhere (*8*). Here we summarize the spectrometer features that are most critical to the experiments described. The millimeter-wave source (Millimeter Wave Oscillator Co., Longmont, CO) produces 220-GHz radiation in a rectangular waveguide that is converted to a circular waveguide mode and launched into a Gaussian beam by a scalar conical horn antenna (ZAX Millimeter Wave Co.). The output of the source is vertically polarized.

The source power is transmitted through a lens beam guide to a semiconfocal cavity consisting of a flat, partially reflective mirror and a spherical mirror. In the transmission mode, radiation is coupled through a small aperture in the spherical mirror, launched from a smooth conical horn, and propagated down a second beam guide.

The detector used for these experiments is a Schottky diode (Millitech Corp., DXW-04) mounted in a short length of rectangular WR-04 waveguide. The Gaussian beam emerging from the beam guide is converted to the appropriate rectangular waveguide mode by a second scalar horn/waveguide transition. The rectangular waveguide thus serves as a polarizing element in front of the detector.

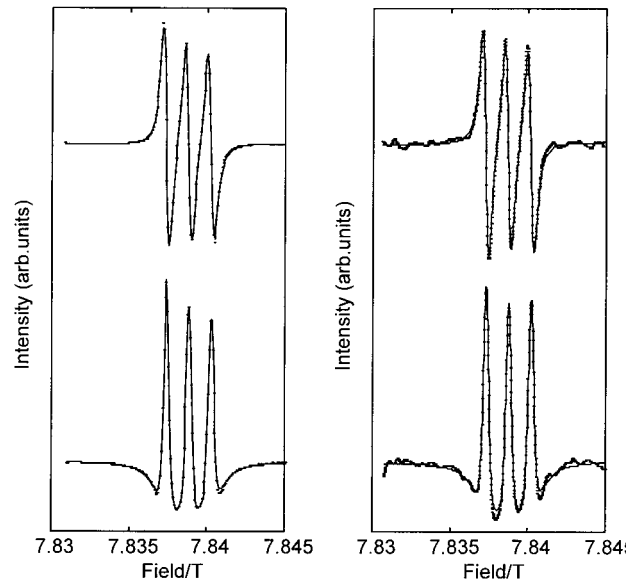

FIG. 4. Representative 220-GHz absorption (top) and dispersion (bottom) spectra of 1 mM Tempone in toluene obtained in transmission (left) and induction (right) modes as described in the text. Solid lines show typical least-squares fits of three Lorentzian lines (Eq. [52]) to the experimental data.

In both transmission and reflection cavities, the liquid sample was held in a cell consisting of two 25-mm-diameter, 0.33-mm-thick quartz windows (Boston Piezo) separated by a 1.6-mm Teflon spacer ring with a 15-mm aperture. The cell assembly was sealed around the edges with epoxy (Torr-Seal, Varian Inc.) and a radial hole was carefully drilled into the center chamber to allow the introduction and removal of sample. The cell was held normal to the beam path in a sleeve between the two mirrors described above and kept in place by a retainer ring.

The sample volume was approximately 300 μL. Since the spectra were obtained in a low-loss solvent, it was not necessary to utilize thin samples or optimize the thickness of either the windows or the sample layer, as has been described previously for aqueous samples (*8, 31*).

Figure 4 shows examples of both absorption and dispersion spectra obtained in transmission mode and by observing the reflected signal in induction mode. Intermediate admixtures of absorption and dispersion could be observed when the phase was adjusted as described below for each of the spectrometer configurations. For comparison with the predictions of the Jones matrix analyses for these circuits, the relative amounts of absorption and dispersion in the spectra were quantified as a function of phase angle adjustment using least-squares analysis as described above. The solid lines in Fig. 4 show typical least-squares fits of Eq. [52] to the experimental data.

Transmission Cavity

In the experiments carried out using the simple transmission cavity design, the input horn of the detector was mounted on a

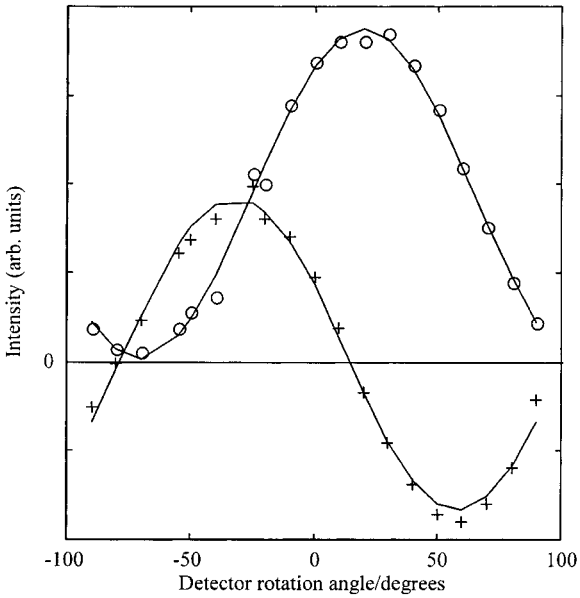

FIG. 5. Relative amplitudes of absorption (circles) and dispersion (crosses) signals as a function of detector rotation measured using a simple transmission configuration with the cavity placed between the source and the detector. Lines indicate least-squares fits as described in the text.

stage that allowed rotation of the detector about the symmetry axis of the horn. Zero rotation was defined to be the orientation at which the rectangular waveguide accepts vertically polarized input (i.e., with the long axis of the waveguide cross-section set horizontal using a bubble level on the case of the detector). Spectra were recorded and the relative contributions of absorption and dispersion determined for a series of different detector orientations.

Figure 5 shows a plot of the unscaled absorption and dispersion coefficients as a function of detector angle rotation θ. The solid lines indicate the least-squares fits of the functions

$$a_A = C_A \sin(2\theta + \phi)$$
$$a_D = C_D[1 + \cos(2\theta + \phi)] \qquad [53]$$

to the data (cf. the $\chi'^{(1)}$ and $\chi''^{(1)}$ coefficients in Eq. [48]). The scale factors C_A and C_D were allowed to vary independently in the fitting procedure.

Induction Spectrometer without Cavity

A similar set of phase measurements was performed using the induction spectrometer arrangement shown in Fig. 3, with the exception that the flat mirror of the sample cavity was omitted to reduce possible phase anomalies due to standing waves (cf. Discussion below). In this mode, the phase difference between the reference signal and the EPR signal was adjusted by moving the rooftop mirror relative to the central grid, which changed the path length of the reference arm. Spectra were recorded as a function of mirror position (with arbitrary zero) and analyzed by least-squares fitting as before. The normalized absorption and dispersion coefficients are plotted in Fig. 6 as a function of rooftop mirror displacement d relative to the central grid of the circuit. Solid lines indicate the least-squares fits of the functions

$$a_A = \cos(kd + \phi)$$
$$a_D = \sin(kd + \phi),$$

with k and ϕ as variable parameters. The phase angle ϕ from the fitting procedure is not meaningful, since it merely specifies the zero of the arbitrary distance scale. The value of k obtained was 9.01 ± 0.07 mm^{-1}, which corresponds to a wavelength of 1.4 mm since the change in path length is twice that of the mirror displacement.

Induction Spectrometer with Cavity

Figure 7a shows one example of the highly skewed phase patterns that may be observed in the presence of a flat cavity mirror. The normalized absorption and dispersion coefficients shown in Fig. 7a were obtained in exactly the same way as that in Fig. 6, with the exception that both of the mirrors around the sample shown in Fig. 3 were present. The cavity was tuned to resonance by moving the spherical mirror so as to minimize the reflected power before the spectra were measured as function of rooftop mirror rotation.

Despite the complicated appearance of the patterns in the presence of the flat mirror, they were quite well fitted by assuming that the bias signal at the mixer consisted of the

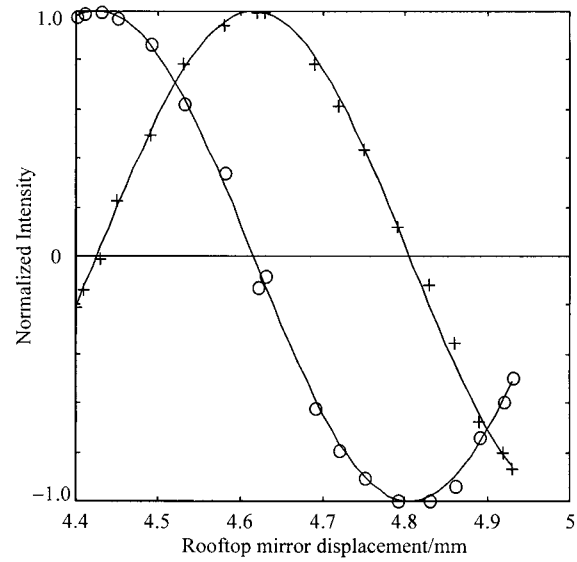

FIG. 6. Relative amplitudes of absorption (circles) and dispersion (crosses) signals as a function of rooftop mirror translation measured using the induction configuration shown in Fig. 3 but omitting the flat partially reflective mirror in the cavity. Lines indicate least-squares fits as described in the text.

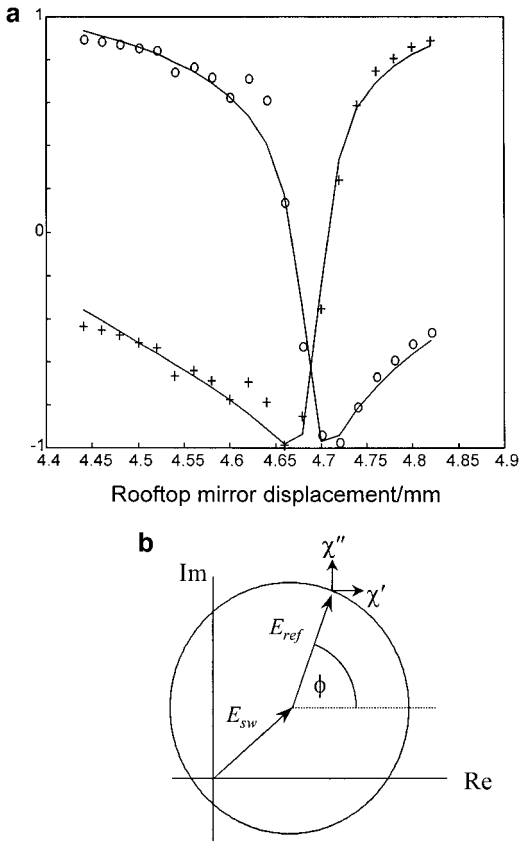

FIG. 7. (a) Relative amplitudes of absorption (circles) and dispersion (crosses) signals as a function of rooftop mirror translation measured using the induction configuration shown in Fig. 3 including the flat partially reflective mirror in the cavity. Lines indicate least-squares fits as described in the text. (b) Phasor diagram showing the relative phases and amplitudes of the reference signal and a standing wave formed by reflection from the cavity. The angle ϕ is varied by changing the position of the rooftop mirror.

reference arm signal added to a standing wave signal with constant phase. Specifically, the solid lines shown in Fig. 7a were calculated using the expressions

$$a_A = \mathrm{Re}\{\mathbf{E}_{sw} + \exp[i(kd + \phi)]\}$$
$$a_D = \mathrm{Im}\{\mathbf{E}_{sw} + \exp[i(kd + \phi)]\},$$

where the reference signal is assumed to have unit magnitude, and the real and imaginary parts of the standing wave vector $\mathbf{E}_{sw}$ were varied separately in the least-squares fitting procedure. The magnitude of $\mathbf{E}_{sw}$ determined from the fit was 0.91 times that of the reference vector, with real and imaginary components of $0.71|\mathbf{E}_{ref}|$ and $0.57|\mathbf{E}_{ref}|$, respectively. The value of k obtained from the curve fitting was identical to that obtained from the data in Fig. 6 to within experimental error. The results are summarized in the form of a phasor diagram in Fig. 7b.

5. DISCUSSION

Phase Discrimination

The experimental results demonstrate that the Jones matrix formalism quite accurately predicts the phase behavior of the two systems investigated. In particular, in transmission mode, the magnitudes of both absorption and dispersion signals exhibit the double-angle dependence on the detector orientation predicted by Eq. [48], including the $\cos(2\theta) + 1$ dependence of the absorption component. Thus, a "negative" absorption signal cannot be observed by adjusting the signal phase in this configuration. It follows that the actual phase of the signal in a transmission mode system, defined as $\tan^{-1}a_A/a_D$, is not given directly by one-half the detector orientation angle.

For the induction mode data, the results display the sinusoidal dependence predicted by Eq. [50] for both the absorption and the dispersion signals. In induction mode, both positive and negative signals may be observed for both the absorption and the dispersion signals.

Transmission Cavity Design

The only single-path spectrometer configuration that permits phase discrimination of the signal is the simplest transmission system consisting of a cavity placed between the source and a polarizing detector. This geometry allows one to discriminate phase without a separate reference signal because the carrier and the EPR signal have different polarizations. Equation [47] shows that the carrier signal is attenuated as the detector polarization is rotated, but its phase remains unchanged. In contrast, for the circularly polarized EPR signal, the apparent phase of the linearly polarized component that is transmitted through a polarizing element may be advanced or delayed by rotating the element, but its magnitude remains unchanged. This makes it possible to vary the effective phase of the EPR signal relative to that of the carrier simply by rotating the detector polarization. Thus, even in the absence of a separate bias signal, a detector with a polarizing element functions as a homodyne mixer in the transmission arrangement, whereas a nonpolarizing device functions as a simple detector.

When the sample in a quasioptical transmission cavity is illuminated with linearly polarized radiation, only half of the incident power is available for magnetic resonance, just as in a conventional waveguide-based sample cavity. One might therefore expect to increase the EPR signal by utilizing the correct circular polarization. This may be accomplished by placing a suitable quarter-wave transformer between the central polarizing grid and the sample cavity, as has been demonstrated by Earle *et al.* (*4*) and Smith *et al.* (*6*). Up to a twofold increase in absolute signal intensity can in principle be realized with this approach, assuming that there are no differences in detector sensitivity or cavity tune in the two configurations.

However, it is important to note that the relative phases of the bias and EPR signals at the detector cannot be controlled

when both are circularly polarized. Jones matrix analysis of configurations employing one or two quarter-wave demonstrates that phase information cannot be retrieved from the transmission mode signal in these cases. For ideal systems, a lock-in detector will measure a pure absorption signal when the signal is illuminated with circular polarization in transmission mode. While this limitation may not seem undesirable, deviations of the cavity from resonance, the presence of higher-order modes in the cavity, and even strong, asymmetric EPR signals can lead to significant admixture of dispersion into the signal. The absence of phase adjustability in such configurations thus significantly limits their utility.

Induction Mode

A major advantage of the induction mode circuit that is apparent from Eqs. [50] and [51] is that the carrier wave reflected from the cavity with coefficient a_R does not appear at the detector in either the vertical or the horizontal polarization. This results from the fact that there is no rotation of the incident beam polarization between the dividing grid and the sample cavity. One consequence of this arrangement is that only one linearly polarized component of the EPR signal reaches the detector. Depending upon the bias characteristics and dynamic range of the detector, this feature may significantly reduce the absolute signal power available at the detector relative to the simple transmission spectrometer. However, such a reduction can be mitigated or even eliminated by the proper choice of detector.

The simplest induction mode design shown in Fig. 3 utilizes fully half of the source power as a bias signal for the detector, which may be unsuitable for many detection schemes. The design can be significantly refined by introducing elements that allow control over the amount of power that is directed along the reference arm, since only a small bias power is needed to operate many homodyne mixers. In place of the dividing grid oriented at $\pi/4$, it is possible to use a dielectric beam splitter (*26*) to divert a small fraction of the power into the reference arm and thus maximize the power in the sample arm. In this case, a separate grid is needed to recombine the signal with the reference beam.

It is also possible to control the reference bias without additional grids by rotating the central grid (cf. Fig. 3). For example, with vertical incident polarization, a grid oriented at about 5° from the horizontal would send approximately 1% (or -20 dB) of the power to the reference arm, which is an appropriate level for low-temperature bolometer mixers. Additional control over the bias power reflected into the detector could be achieved by rotating the axis of the rooftop mirror. These additional adjustments are easily accounted for in the Jones matrix expressions by utilizing the general matrix forms given in Eqs. [38] and [39] for arbitrary orientations of these elements.

A second important characteristic of the induction mode design is that the ESR signal component at frequency ω_m appears with opposite signs in the vertical and horizontal polarizations, whereas the reference signal appears with the same sign. This feature lends itself conveniently to a balanced mixer design in which two matched mixers are set to measure in the vertical and horizontal directions and the signals are electronically subtracted. The signal intensity can thus be doubled with such an arrangement, while AM noise from the source is largely suppressed.

When all of the above factors are considered, the induction mode configuration emerges as perhaps the most useful design for general work. Smith *et al.* (*5, 6*) have described an induction spectrometer that combines many of the advantages of individual components discussed above. The design functions in essentially the same way as the spectrometer shown in Fig. 3, but incorporates a number of significant refinements of this basic design that minimize stray reflections and standing waves. The greatly decreased noise sensitivity in the induction arrangement more than compensates for the reduced signal intensity at the detector.

Standing Waves

The presence of standing waves in the system can dramatically alter the simple sinusoidal dependence of the absorption and dispersion signal intensities predicted by the basic Jones matrix formalism, as shown in Fig. 7a. Presumably, standing waves arise between an imperfectly matched cavity and other partially reflective elements in the transmission circuit. Although it is difficult to extend the formalism itself to account for such effects waves explicitly, the basic result can be combined with the appropriate vector analysis to identify and characterize adventitious signals in the system. In this way, an EPR cavity containing a well-characterized sample can be made to serve as an *ad hoc* vector analyzer.

Perhaps the most important effect of strong system standing waves is on the spectrometer sensitivity. As noted in Appendix 2 of Ref. (*6*), even small deviations of the cavity frequency from resonance can lead to a significant amount of conversion of FM noise from the source to AM noise at the detector. Variations in the cavity Q appear as changes in the coefficients a_R and a_T (as well as the much smaller b_R and b_T terms) in the Jones matrix expressions. One of the major causes of such deviations is microphonic vibration of the cavity mirrors or sample due to Lorentz forces on the field modulation coils, which can be quite large at high magnetic fields.

Microphonic vibrations can lead to direct modulation of the carrier signal, so that the terms depending on a_R and a_T in the Jones matrix expressions have a $\sin(\omega_m t)$ dependence that appears in the signal at the lock-in amplifier. In addition to generating greater noise, these effects produce a large baseline offset that limits the dynamic range of the lock-in amplifier. Thus, circuit arrangements that allow a significant amount of power reflected from the cavity to reach the detector may be

much more susceptible to noise than circuits which isolate the cavity from the detector, leading to lower sensitivity despite the apparently larger signal intensity.

Comparison with Alternative Treatments

We now briefly compare the Jones matrix derived for a quasioptical reflection cavity to recent results from an alternative type of cavity analysis (*6, 32*). The essence of the approach is to construct a set of field equations for the resonator based upon the reflection, transmission, and absorption coefficients of the cavity elements, including the EPR sample. One can then solve for the incident and reflected fields as well as for the field circulating in the cavity.

The shunt transmission cavity analyzed by Barnes and Freed (*32*) in this way allows the coupling parameter for the cavity to be varied by adjusting the spacing between a pair of dielectric beam splitters in the center of the cavity. The second major feature of the cavity is that the spherical cavity mirrors are placed along an axis perpendicular to the direction of the incident beam. This geometry allows planar samples such as aligned membranes to be placed with their normal axis perpendicular to the spectrometer field. Despite the significant differences in the geometry of the shunt transmission cavity from the Fabry–Perot geometry utilized in most high-frequency spectrometers, the results of their analysis correspond directly with the Jones matrix given for a quasioptical transmission cavity in Eq. [34]. For the particular design described by Barnes and Freed, β_1 and β_2 in Eq. [34] would be essentially equal.

Smith *et al.* (*6*) have presented a similar cavity field analysis for the basic Fabry–Perot resonator. One of their major conclusions was that the magnitude of the cross-polar signal from a cavity illuminated with plane-polarized radiation has a field strength similar to that of the copolar signal if the reflectivity of the coupling mirror is the same for both linear states. This result follows immediately from an examination of Eq. [35], which is the Jones matrix expression for a reflection cavity in which the coupling mirror has a reflectivity that is independent of the incident polarization state.

Also treated in the analysis of Smith *et al.* is the case of a cavity in which one of the mirrors is polarizing. In this case, the field analysis shows that the cross-polar signal is obtained with a sensitivity proportional to $(Q_L)^{1/2}$, where Q_L is defined in terms of the coupling parameter for the mirror in the copolar direction. The corresponding Jones matrix for this case may be derived by analogy with the equivalent circuit analysis given by Portis and colleagues (*16, 33*).

$$\begin{pmatrix} R_V \\ R_H \end{pmatrix} = \begin{pmatrix} i\dfrac{\beta Q_L}{(1+\beta)}\eta\chi & \left(\dfrac{\beta Q_L}{1+\beta}\right)^{1/2}\eta\chi \\ -\left(\dfrac{\beta Q_L}{1+\beta}\right)^{1/2}\eta\chi & -i\eta\chi \end{pmatrix} \begin{pmatrix} A_V \\ A_H \end{pmatrix} \quad [54]$$

Perhaps surprisingly, this result shows that the magnitude of the signal is the same regardless of whether one excites parallel and observes perpendicular to the mirror polarization or excites perpendicular and observes parallel to it. In the former case, the cavity amplifies the millimeter-wave power, whereas in the latter, the cavity amplifies the EPR signal itself.

Such a cavity might be useful in time-domain spectrometers where isolation of the detection circuitry from high-powered source pulses is desired. It could also be utilized as a variable-coupling cavity by rotating the orientation of the polarizing mirror with respect to the input polarization. The general form for such a Jones matrix would then be given by a coordinate transformation, by analogy with the other polarizing elements discussed above.

Limitations and Possible Extensions of the Jones Matrix Formalism

We now briefly examine some of the major assumption of the Jones matrix formulations in order to assess their validity for practical applications, and we briefly indicate how the formalism may be adjusted to compensate for them. The first, and probably the most important, assumption is that the two linear polarization states in the cylindrical cavity are well isolated ($>$30 dB). Problems may arise if cross-polar modes are excited by the quasioptical elements used to couple radiation into the cavity. Since polarizing elements with at least 30 dB of isolation are readily available, this is usually a negligible effect. However, the sample itself may scatter the incident power into the orthogonal mode by mechanisms other than magnetic resonance. These effects can in general be modeled by including additional off-diagonal terms in the Jones matrices for the cavities that couple the two orthogonal linear modes.

A second major assumption of the formalism is that there is a single resonant mode inside of the cavity, specifically the fundamental mode of a Gaussian beam. Mode impurities in the input beam, irregularities in sample geometry, scattering from irises or imperfections in the cavity mirrors, and aperture effects can all cause coupling into higher radial modes of the cavity. Such modes tend to have field distributions over a larger effective diameter than the fundamental mode with nodes near the sample region. More importantly, higher modes can differ in phase from the fundamental so that electron spins which interact primarily with a higher radial mode may produce an EPR signal with a significantly different phase from that of the carrier wave. (We have accidentally observed this effect in liquid samples that developed a large bubble near the center of the cavity where the field amplitude of the fundamental mode is concentrated.) In principle, this type of effect could be handled by constructing a Jones matrix for each of the relevant higher order modes and utilizing a scattering matrix to introduce coupling between the modes. In practice, however, it should generally be more effective to adjust the signal phase at the detector to compensate for mode impurities.

The third major assumption of the formalism presented above is that the cavity is tuned to its resonant frequency and that the magnetic resonance causes only a small deviation from this condition. The implications of this assumption for system noise performance have been considered above. Here we note that certain types of cavity detuning can also introduce phase shifts in the signal that are not explicitly accounted for by the formalism. Displacement of the cavity mirrors from their positions at perfect tune can change the phase of the complex-valued cavity reflection coefficient, which may influence the apparent phase of the EPR signal. Similarly, displacement of a lossy sample from a node of the E field in the cavity may introduce phase shifts that are not accounted for in the Jones matrix formalism. Both of these effects may be taken into account using a transfer matrix analysis of the cavity elements, including the windows of the sample cell and the lossy dielectric layer containing the sample.

Finally, in the absence of automatic frequency control the shift in effective cavity frequency at EPR resonance can detune the cavity enough to introduce a significant dispersion component for very strong signals. Phase anomalies caused by mirror or sample displacement may readily be corrected by adjusting the signal phase at the detector. One possible solution for the third type of artifact is to implement automatic frequency control (AFC) as is used at lower EPR frequencies (*34*, *35*) or an analogous scheme to lock the quasioptical cavity to the incident source frequency. The majority of high-field EPR spectrometers described in the literature do not have such a feature, although a recently reported design utilizes the Faraday rotator scheme to monitor the power reflected from the cavity for feedback into an AFC loop (*6*).

CONCLUSION

An extension of the basic Jones matrix formalism to high frequency, quasioptical EPR has been presented, and the strict analogies between this method and the standard representation used for conventional EPR circuits have been demonstrated. The two spectrometer configurations most commonly used in quasioptical systems, namely the simple transmission mode and the induction mode, were analyzed using the formalism. Experimental tests of the phase performance of each configuration at 220 GHz verify the predictions of the analysis. The effect of standing wave anomalies on the phase performance of reflection cavity designs is also illustrated experimentally. The formalism can usefully be integrated into a general analysis of spectrometer performance and sensitivity and also serves to identify methods for achieving phase discrimination using standard homodyne mixer detection schemes.

ACKNOWLEDGMENTS

This work was supported by NSF CAREER Award MCB 9600940. K.A.E. acknowledges support of this work through NSF Grant CHE-9615910 and NIH Grant RR07126-07. The resources of the Cornell Theory Center aided in the analysis of several of the spectrometer configurations reported on here. We thank Dr. Stephen Kolaczkowski for assistance in assembling the different configurations used under Experimental. Useful discussions with Professors Jack H. Freed, Paul F. Goldsmith, and Graham M. Smith are also gratefully acknowledged.

REFERENCES

1. W. B. Lynch, K. A. Earle, and J. H. Freed, A 1 millimeter-wave ESR spectrometer, *Rev. Sci. Instrum.* **59,** 1345–1351 (1988).
2. D. E. Budil, K. A. Earle, W. B. Lynch, and J. H. Freed, EPR at 1 mm wavelengths, *in* "Advanced EPR: Applications in Biology and Biochemistry" (A. J. Hoff, Ed.) pp. 307–338, Elsevier, Amsterdam (1989).
3. F. Mueller, M. A. Hopkins, N. Coron, M. Grynberg, L. C. Brunel, and G. Martinez, A high magnetic field EPR spectrometer, *Rev. Sci. Instrum.* **60,** 3681–3684 (1989).
4. K. A. Earle, D. S. Tipikin, and J. H. Freed, Far infrared EPR spectrometer utilizing a quasi-optical reflection bridge, *Rev. Sci. Instrum.* **67,** 2502–2513 (1996).
5. G. M. Smith, J. C. G. Lesurf, R. H. Mitchell, and P. C. Riedi, A high-performance mm-wave electron spin resonance spectrometer, *IEEE MTT-S Digest* 1677–1680 (1995).
6. G. M. Smith, J. C. G. Lesurf, R. H. Mitchell, and P. C. Riedi, A quasioptical cw mm-wave ESR spectrometer, *Rev. Sci. Instrum.* **69,** 3924–3937 (1998).
7. K. A. Earle, D. E. Budil, and J. H. Freed, Millimeter wave electron spin resonance using quasioptical techniques, *in* "Advances in Magnetic and Optical Resonance" (W. S. Warren, Ed.), Vol. 19, Ch. 3, Academic Press, New York (1996).
8. J. Cardin, J. R. Anderson, S. V. Kolaczkowski, and D. E. Budil, Quasioptical design for an EPR spectrometer based on a horizontal bore superconducting solenoid, *Appl. Magn. Reson.* **16,** 273–292 (1999).
9. M. Rohrer, J. Krzystek, V. Williams, and L.-C. Brunel, Fabry–Perot resonator for high-field multifrequency ESR at millimetre and submillimetre wavelengths, *Meas. Sci. Technol.* **10,** 275–294 (1999).
10. M. R. Fuchs, T. F. Prisner, and K. Moebius, A high-field/high-frequency heterodyne induction-mode electron paramagnetic resonance spectrometer operating at 360 GHz, *Rev. Sci. Instrum.* **70,** 3681–3683 (1999).
11. E. J. Reijerse, P. J. van Dam, A. A. K. Klaassen, W. R. Hagen, P. J. M. van Bentum, and G. M. Smith, Concepts in high-frequency EPR—Applications to bio-inorganic systems, *Appl. Magn. Reson.* **14,** 153–167 (1998).
12. A. Ivancich, T. A. Mattioli, and S. Un, Effect of protein microenvironment on tyrosyl radicals. A high-field (285 GHz) EPR, resonance Raman, and hybrid density functional study, *J. Am. Chem. Soc.* **121,** 5743–5753 (1999).
13. J. C. G. Lesurf, "Millimetre-Wave Optics, Devices, and Systems," Hilger, Bristol (1990).
14. C. P. Poole, "Electron Spin Resonance: A Comprehensive Treatise on Experimental Techniques," 2nd ed., Wiley, New York (1979).
15. T. H. Wilmshurst, W. A. Gambling, and D. J. E. Ingraham, Sensitivity of resonant cavity and travelling-wave ESR spectrometers, *J. Electron. Contr.* **13** (1962).
16. D. T. Teaney, M. P. Klein, and A. M. Portis, Microwave superheterodyne induction spectrometer, *Rev. Sci. Instrum.* **32,** 721–729 (1961).

17. C. G. Montgomery, R. H. Dicke, and E. M. Purcell, "Principles of Microwave Circuits," pp. 99–120, McGraw–Hill, New York (1948).
18. K. Schuster, Anwendung der Vierpoltheorie auf die Probleme der optischen Reflexionsminderung, Reflexionverstärkung und der Interferenzfilter, *Ann. d. Physik. 6e Reihenfolge* **4,** 352–356 (1948).
19. D. H. Martin and J. Lesurf, Submillimetre-wave optics, *Infrared Phys.* **18,** 405–412 (1978).
20. Deleted in proof.
21. A. F. Harvey, "Microwave Engineering," pp. 889–892, Academic Press, London (1963).
22. R. E. Collin, "Foundations for Microwave Engineering," 2nd ed., Chap. 3–5, McGraw–Hill, New York (1992).
23. M. Born and E. Wolf, "Optics," 6th ed., pp. 51–70, Pergamon, Oxford (1980).
24. K. C. Gupta, R. Garg, and R. Chadha, "Computer-Aided Design of Microwave Circuits," Chap. 2.1, Artech House, Dedham, MA (1981).
25. R. Ulrich, Far-infrared properties of metallic mesh and its complementary structure, *Infrared Phys.* **7,** 37–55 (1967).
26. P. F. Goldsmith, Quasioptical techniques at millimeter and submillimeter wavelengths, *in* "Infrared and Millimeter Waves" (K. J. Button, Ed.), Vol. 6, pp. 277–344, Academic Press, New York (1982).
27. A. Abragam and B. Bleaney, "Electron Paramagnetic Resonance of Transition Ions," Clarendon Press, Oxford (1970).
28. W. G. Chambers, A. E. Costley, and T. J. Parker, Characteristic curves for the spectroscopic performance of free-standing wire grids at millimeter and submillimeter wavelengths, *Int. J. Infrared Millimeter Waves* **9,** 157–172 (1988).
29. O. E. Myers and E. J. Putzer, Measurement broadening in magnetic resonance, *J. Appl. Phys.* **30,** 1987–1991 (1959).
30. D. H. Martin and E. Puplett, Polarized interferometric spectroscopy for the millimetre and submillimetre spectrum, *Infrared Phys.* **10,** 105–109 (1969).
31. J. P. Barnes and J. H. Freed, Aqueous sample holders for high-frequency electron spin resonance, *Rev. Sci. Instrum.* **68,** 2838–2846 (1997).
32. J. P. Barnes and J. H. Freed, A "shunt" Fabry–Perot resonator for high-frequency electron spin resonance utilizing a variable coupling scheme, *Rev. Sci. Instrum.* **69,** 3022–3027 (1998).
33. K. A. Earle, "Magnetic Resonance Relaxation Studies in High Magnetic Fields," Ph.D. Dissertation, Cornell Univ. (1994).
34. I. B. Goldberg and H. R. Crowe, Effect of cavity loading on analytical electron spin resonance spectroscopy, *Anal. Chem.* **49,** 1353 (1977).
35. P. Ludowise, S. S. Eaton, and G. R. Eaton, A convenient monitor of EPR automatic frequency control function, *J. Magn. Reson.* **93,** 410–412 (1991).